Journal of Materials Chemistry C

ROYAL SOCIETY OF CHEMISTRY

PAPER

View Article Online
View Journal | View Issue



Check for updates

Cite this: J. Mater. Chem. C, 2021, 9, 16516

# Synthesis, phase purification and magnetic characterization of the $(Cr_{1-x}, Mn_x)_2AlC$ MAX-phase†

Kirill Sobolev,*[a] Hanna Pazniak,*[b] Michael Farle,[bc] Valeria Rodionova[a] and Ulf Wiedwald*[b]

Received 2nd July 2021,
Accepted 23rd October 2021

DOI: 10.1039/d1tc03092b

rsc.li/materials-c

The $Cr_2AlC$ MAX phase is a promising parent compound to introduce magnetism to nano-laminated ternary carbides by doping with Mn. Here, we demonstrate that Mn doping of bulk $Cr_2AlC$ powder synthesized by arc melting results in incorporation up to 16 at% Mn in the M-layers of the MAX phase. Simultaneously, the relative amount of secondary phases is overall low, however, increases with Mn doping. We successfully applied chemical treatment in dilute hydrochloric acid to eliminate secondary phases and studied the magnetic properties before and after treatment by magnetometry between 3 K and 800 K. All MAX-phases show a paramagnetic response.

## Introduction

MAX phases are the family of nano-lamellar compounds sharing the chemical formula $M_{n+1}AX_n$, where M is an early transition metal, A is a main group element (mostly of groups 13–15) and X is either C or N.[1] The MAX phases ($Ti_2SC$ and $Zr_2SC$) were initially demonstrated by Kudielka and Rohde[2] and further synthesized by Jeitschko and Nowotny[3] in the 1960s, however attracted more attention in the 2000s, after the pioneering work of Barsoum and coworkers.[1] MAX phases combine the characteristic properties of both, metals and ceramics; MAX-phases are highly electrically and thermally conductive, elastically stiff and machinable like metals. In addition, they can withstand high temperatures, and are tolerant to high-temperature corrosion and harsh environments, like ceramics.[1] Such a unique set of properties originates from the peculiar atomically layered crystal structure, consisting of alternating layers of $M_6X$ octahedra and A atoms (space group $P6_3/mmc$).[1] Hence, MAX-phases are being considered for a plethora of practical applications, from chemically stable electrical contacts to protective and shielding coatings, especially for high-temperature applications.[4] MAX-phases can be also chemically etched, removing the relatively weakly-bonded A element, to form two-dimensional materials named MXenes, first discovered by Gogotsi, Naguib, *et al.* a decade ago.[5] Since then, MXenes gained even more attention than their parental MAX-phases due to the huge expansion of possible application of 2D materials towards flexible electronics, energy accumulation, environmental issues and biomedicine.[6] Nowadays, except the common ternary $M_{n+1}AX_n$ phases, quaternary doped MAX-phases are being widely studied. This is possible since MAX-phases form either stable solid solutions on M-,[7,8] A-[7–9] and X- sites[10] or stable phases in out-of- ($(M',M'')_{n+1}AlC_{n'}$) and in-plane $\left(\left(M'_{2/3}, M''_{1/3}\right)_2AlC\right)$ chemically ordered compounds, denoted as o-MAX and i-MAX phases, respectively.[11,12] Such a variety of possible compositions and atomic arrangements allows for the tailoring the physical properties and functionalities of MAX-phases.

One of the goals of MAX-phase doping is the synthesis of stable magnetic MAX-phases to expand their usage towards spintronics, functional oxidation resistant and wear resistant magnetic coatings[13] or even more intriguing as a precursor for the synthesis of magnetic MXenes.[14,15] Among the ternary MAX-phases, only $Mn_2GaC$ shows long-range magnetic ordering up to now.[16–18] This material has a first order magnetic phase transition at about 210 K from an antiferromagnetic (AFM) at higher temperatures to the non-collinear AFM spin state and a high Néel temperature of 507 K.[17] The potential to tune such magnetic transitions in quaternary MAX-phases by doping with a 4th element is one of the main ideas underlying the search of magnetism in such systems. Up to date, magnetic quaternary MAX-phases were obtained *via* doping with rare-earth elements (namely, $(Mo_{2/3}Tb_{1/3})_2AlC$ and $(Mo_{2/3}Er_{1/3})_2AlC$

[a] Immanuel Kant Baltic Federal University, 236041, Kaliningrad, Russian Federation. E-mail: kirill_sobolev-off@mail.ru
[b] Faculty of Physics and Center for Nanointegration Duisburg-Essen (CENIDE), University of Duisburg-Essen, 47057 Duisburg, Germany. E-mail: hanna.pazniak@uni-due.de, ulf.wiedwald@uni-due.de
[c] Kirensky Institute of Physics, Federal Research Center KSC SB RAS, Krasnoyarsk, 660036, Russian Federation

† Electronic supplementary information (ESI) available. See DOI: 10.1039/d1tc03092b

compounds[19]) and doping with manganese ($(Mo_{1/2}Mn_{1/2})_2GaC$, $(Cr,Mn)_2GaC$, $(Cr,Mn)_2GeC$, *etc.*[20–22]).

The $(Cr_{1-x}Mn_x)_2AlC$ MAX-phase already caught attention due to its possible magnetic long-range order following the above strategy. In the first theoretical study of Dahlqvist $(Cr_{1-x}Mn_x)_2AlC$ MAX-phase was predicted to be ferromagnetic.[23] However, when several different antiferromagnetic spin states were considered, it was shown that the lowest total energy of the $(Cr_{1-x}Mn_x)_2AlC$ MAX-phase is reached for an in-plane AFM order with a very small energy difference with respect to the FM spin state.[24] To reliably understand the magnetism in this compound substantial issues had to be solved. Firstly, the $(Cr_{1-x}Mn_x)_2AlC$ MAX-phase demonstrated strong degradation of the sample's phase quality and purity upon the incorporation of Mn on Cr sites.[25,26] Secondly, Mn atoms tend to poorly intermix into the MAX-phase structure, leading to a total doping level, not higher than 10 at% for bulk samples.[27] Recently, a protocol to produce pure-phase samples of $(Cr_{1-x}Mn_x)_2AlC$ MAX-phase was established pushing the limit of Mn doping level to about 18 at%.[28]

Herein, we exploit this protocol to synthesize a series of samples of $(Cr_{1-x}Mn_x)_2AlC$ MAX-phases with Mn contents $0 < x < 0.16$. The chosen synthesis approach – arc melting technique – gives possibility for such an increment of the dopant content in the MAX-phase, analogous to what has been demonstrated for the arc deposited $(Cr_{1-x}Mn_x)_2AlC$ thin films by Mockute *et al.*[29] We comprehensively investigate their magnetic properties at low (down to 3 K) and high (up to 800 K) temperatures. It turns out that small amounts of side phases hinder the magnetic characterization. Thus, we establish a protocol for chemical treatment of the samples to effectively remove these side phases allowing the magnetic characterization of almost phase-pure MAX-phases. The detailed magnetic analysis of purified $(Cr_{1-x}Mn_x)_2AlC$ with $x$ up to 0.16 revealed paramagnetic response. We determine the magnetic susceptibility as a function of dopant concentration. The sample processing and findings in the present work are important for the understanding and determination of the side phase's impact on the magnetic properties of bulk MAX-phases.

## Experimental section

Polycrystalline bulk samples of the $(Cr_{1-x}Mn_x)_2AlC$ MAX-phase with nominal manganese concentration of $x$ = 0, 0.1, 0.2 and 0.25 were synthesized by arc melting using the optimized protocol as discussed elsewhere.[30] Elemental powders of chromium Cr (99.95% purity), manganese Mn (99.95% purity), aluminum Al (99.999% purity) and chromium carbide $Cr_3C_2$ (99.95% purity) were all supplied from GIRMET (Moscow, Russian Federation). In total, 3 g of initial compounds were placed into a water-cooled copper crucible, keeping $(2 - x) : x : 1.2 : 1$ stoichiometry of Cr : Mn : Al : C. This stoichiometry was suggested in our previous work as optima to produce single-phase parent $Cr_2AlC$ MAX phase.[30] The melting was conducted in an Arcast furnace using a Miller XMT 450 CC/CV power supply under high purity (99.9998%) argon atmosphere, the argon pressure was set to 10 bar. After melting, samples were annealed in a muffle furnace ITM-10.900 in an evacuated quartz tube at 900 °C for 120 h to promote homogeneity. Samples were heated at a rate of $\sim$40 K min$^{-1}$ and then cooled down freely.

As-cast samples were pre-checked by scanning electron microscopy/energy dispersive X-ray (SEM-EDX) analysis to observe the resulting phase composition. A Quanta FEG 250 scanning electron microscope with EDAX Apollo X EDX-detector was used to visualize the microstructure and to measure the chemical compositions in each of the observed phases. The resulting Mn doping level for the studied $(Cr_{1-x}Mn_x)_2AlC$ MAX-phase was also determined from EDX analysis. A copper reference sample was used for the calibration before carrying out EDX measurements. To perform SEM-EDX analysis, samples were cut with a diamond circular saw to obtain cross-sections. These parts were fixed in epoxy resin, grinded and polished with SiC abrasive paper down to 2500 grit and with diamond pastes down to 1 μm.

Afterwards, the samples were grinded to powders with maximum 200 μm particle size by mechanical grinding in an agate pounder. The powders (approx. 1 g) were treated with 10% HCl aqueous (approx. 10 ml) solution Sigma Aldrich H1758 (36.5–38.0%) for 20 min at room temperature under continuous magnetic stirring. After the chemical treatment, the powders were washed using ultra-high purity water to eliminate residual reaction products, which are mainly salts, by means of centrifugation (Eppendorf 5810). Before and after the chemical treatment the powders were examined by X-Ray Diffractometry (XRD). XRD analysis was performed using a Malvern Panalytical X'Pert MPD PW3040 diffractometer (Cu anode, $\lambda$ = 0.15418 nm) in 10°–120° 2$\theta$-range with steps of 0.002°.

Samples for the transmission electron microscopy (TEM) were prepared by fine grinding of sample powder and its further sonication in an ultrasonic bath in absolute ethanol for 1 hour. The dispersion was drop casted on a lacey carbon grid. EDX spectra and elemental mapping have been recorded using JEOL 2200FS microscope equipped with Oxford X-Max 80 mm$^2$ detector.

The magnetic properties of the powder samples before and after chemical treatment were studied by vibrating sample magnetometry in a Physical Property Measurement System (PPMS) DynaCool in fields of ±90 kOe and a variable temperature between 2–800 K. Approximately 10 mg of powder were weighed and placed inside synthetic capsules for low and ambient temperature measurements. Magnetization *versus* temperature (*M vs. T*) curves were obtained according to a zero-field-cooled/field-cooled (ZFC-FC) protocol in the temperature range from 3 K to 400 K in presence of external magnetic fields of 100 Oe and 1000 Oe. Hysteresis loops (*M vs. H*) were obtained at fixed temperatures $T$ = 3 K, 5 K, 10 K, 30 K, 50 K, 100 K, 200 K and 300 K in magnetic fields up to 90 kOe. At elevated temperatures, the sample powder has been mixed with Zircar cement and pasted on a heating holder. High temperature *M vs. T* curves were obtained according to field-warmed/field cooled (FW-FC) protocol in the temperature range from

300 K to 800 K in presence of an external magnetic field of 1000 Oe. Since the exact amount of powder cannot be precisely determined, the high temperature signal has been scaled to the low temperature magnetization (3–400 K) using the overlapping temperature range 300–400 K.

## Results and discussion

### Structural characterization

The microstructure of the as-cast samples of $(Cr_{1-x}Mn_x)_2AlC$ MAX-phase with the nominal content of Mn $x$ = 0, 0.1, 0.2 and 0.25 is presented in Fig. 1. The SEM micrographs clearly show that the synthesized samples are not phase pure due to the presence of different contrast in the images, acquired in the back scattered electron (BSE) mode. To identify the phases, EDX analysis using at least 7 different points of each phase is performed and averaged (Fig. 1 and Table S1, ESI†). The sample with $x$ = 0 (Fig. 1a) contains two main phases: the $Cr_2AlC$ MAX-phase, identified by elongated grey grains with a characteristic Cr : Al ratio close to 2 : 1, and an $Al_8Cr_5$-type intermetallic compound, occupying intergrain regions with darker contrast.[30]

Upon adding Mn (Fig. 1b–d), the MAX-phase remains as the predominant phase, while the by-product phase changes its chemical composition with increasing Mn content. This can be followed by the changing contrast of secondary phase in Fig. 1 and resulting stoichiometries by EDX (Table S1, ESI†). According to the EDX analysis at a highest nominal Mn content of $x$ = 0.25, the $Mn_3AlC$ antiperovskite structure, enriched by Cr is crystallized (light grey region Fig. 1d and Table S1, ESI†). The coexistence of a $Mn_3AlC$ phase in the highly Mn-doped MAX phase was previously reported by Mockute *et al.*[31] and confirmed by qualitative XRD analysis (Table S2, ESI†).

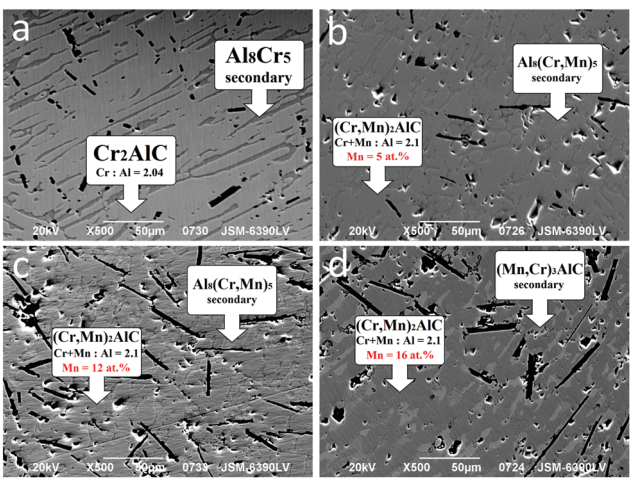


Fig. 1 Representative BSE-SEM images of $(Cr_{1-x}Mn_x)_2AlC$ MAX-phase with the nominal concentration of Mn $x$ = 0, 0.1, 0.2 and 0.25 (a to d, respectively). Chemical compositions of the observed phases (MAX-phase and secondary phases) are indicated in the SEM images as determined by EDX analysis.

Based on the EDX analysis, the actual amount of Mn in the $Cr_2AlC$ MAX-phase structure is 5.3 at%, 12.2 at% and 15.7 at% for samples with 10, 20 and 25 at% nominal Mn doping, correspondingly (Table S1, ESI†). Point-by-point EDX detection demonstrates the homogeneous distribution of Mn in the samples volume. Since the Cr content in the chemical composition of the Mn-doped MAX phase is reduced while increasing the Mn content, keeping the (Cr + Mn) : Al ratio close to 2 : 1 at the same time, we suggest the successful substitution of Mn for Cr. Since even small amounts of secondary phases could significantly impact on the magnetic properties, easily leading to misinterpretation, the synthesized MAX-phases were grounded to fine powders (less than 200 μm) and chemically etched to eliminate impurities of secondary phases. We used 10% HCl as chemical etchant and treated the powder as described in the Materials and Methods section. As a result, water-soluble $Al^{+3}$, $Mn^{(+2,+3)}$ and $Cr^{(+2,+3)}$ chlorides are formed. Since the treatment is performed in aqueous environment, the oxygen could be easily attached to the surface of intermetallics. The chemical treatment does not influence the morphology or chemistry of the MAX-phase, which is proven by the SEM-EDX results (Fig. S1, ESI†), demonstrating the original well-defined layered structure and characteristic 2 : 1 : 1 stoichiometry of $Cr_2AlC$.

The success of chemical treatment on the phase purity of Mn-containing samples is judged by comparing the $x$ = 0.16 sample before and after the purification procedure in Fig. 2. The data demonstrates that the as-cast sample shows all expected diffraction peaks of the MAX-phase and a $Mn_3AlC$ side phase pattern. The diffractogram shows a slight shift towards lower $2\theta$ angles as compared to the $Mn_3AlC$ reference pattern which is due to Cr atoms partially incorporated into the perovskite structure. This finding is also confirmed by the EDX measurements (Fig. 1 and Table S1, ESI†). After chemical treatment, the XRD pattern shows MAX-phase peaks, while the perovskite phase pattern completely vanished. The purity of the MAX phase powder is significantly improved following the treatment recipe.

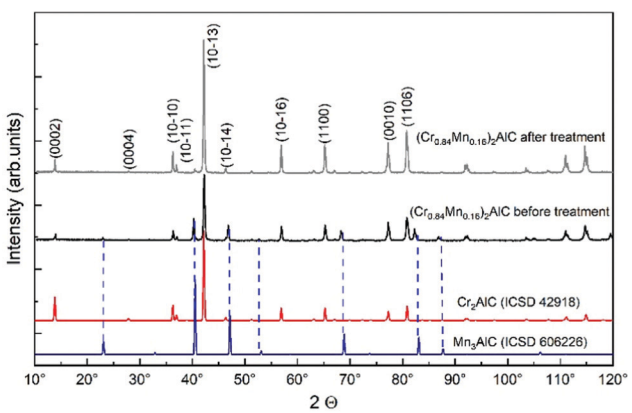


Fig. 2 XRD patterns of the $(Cr_{0.84}Mn_{0.16})_2AlC$ MAX-phase before and after chemical treatment. The reference database XRD patterns of $Cr_2AlC$ and $Mn_3AlC$ are placed below for comparison.

Fig. 3 presents the XRD patterns of the sample series of compositions with $x$ = 0, 0.05, 0.12, and 0.16 after chemical treatment. The XRD patterns of chemically treated powders demonstrate the presence of all characteristic MAX-phase peaks with one additional minor peak at around 41.5° that is attributed to the $Cr_7C_3$ side phase. For the synthesized compositions, the calculated $a$ lattice parameter of 0.285 ± 0.004 nm and the $c$ lattice parameter of 1.275 ± 0.004 nm are almost unchanged when Mn substitutes Cr. This behavior has already been experimentally demonstrated for the $(Cr_{1-x}Mn_x)_2GeC$ system.[32] Local elemental mapping by EDX-STEM on the 100 nm scale of a representative grain in $(Cr_{0.84}Mn_{0.16})_2AlC$ is presented in Fig. 4.

The elemental maps further support the presence of Mn in the structure and its homogeneous distribution. The calculated chemical composition of Mn is 0.15–0.16, which agrees well with the SEM findings above. However, based on the performed EDX-analysis results we cannot unambiguously claim the homogeneity of Mn distribution on the local level in the whole sample volume or clearly distinguish the presence of Mn-rich and Mn-poor regions, suggested by Tao *et al.*[33] In summary, the structural characterization, performed on phase purified powders, suggests that the synthesized materials are phase pure and well suited for the further magnetic characterization.

### Magnetic characterization

The influence of the chemical treatment of MAX-phases on the magnetic properties is shown in Fig. 5a for the $(Cr_{0.84}Mn_{0.16})_2AlC$ MAX-phase sample. Obviously, chemical treatment leads to a drastic decrease of the magnetization. The magnetization drops by more than 50% at temperatures of $T$ = 3 K and $T$ = 300 K and by more than one order of magnitude near $T$ = 80 K. The splitting of ZFC–FC curves of the as-cast sample disappears after chemical treatment together with the apparent bend of the curve near $T$ = 80 K. Thus, we associate these features to the magnetic response of side phases which are eliminated by the chemical treatment. Consideration of the impact of side phases on the overall magnetic signal of the sample is reasonable as it was discussed in the review paper of Ingason[13] and addressed in various experimental works.[19,27] The feature at $T$ = 80 K is likely due to the $(Mn, Cr)_3AlC$ antiperovskite side phase that was observed by both SEM and XRD measurements. The parent $Mn_3AlC$ is a ferromagnet with the Curie point close to room temperature,[34] however, the Cr doping on Mn sites may easily shift the ordering temperature downwards. At the same time, the curve splitting at low temperatures can be associated with minor

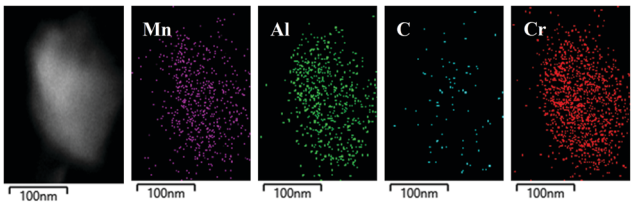


Fig. 4 EDX-STEM image of a grain from the $(Cr_{0.84}Mn_{0.16})_2AlC$ sample and corresponding elemental mappings of Mn, Al, C and Cr.

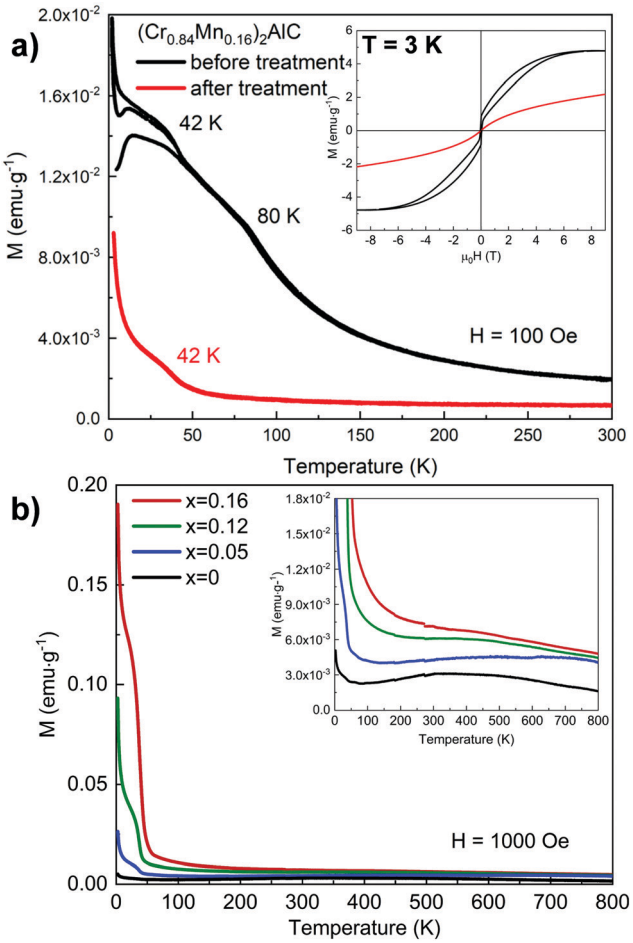


Fig. 5 (a) $M$ *vs.* $T$ curves for the $(Cr_{0.84}Mn_{0.16})_2AlC$ MAX-phase sample in 100 Oe before and after chemical treatment. The inset shows hysteresis loops at $T$ = 3 K before and after purification; (b) $M$ *vs.* $T$ dependencies for $(Cr_{1-x}Mn_x)_2AlC$ MAX-phase samples with $x$ = 0, 0.05, 0.12, and 0.16 in $H$ = 1000 Oe after chemical treatment. The inset enlarges the magnetic signal over the entire temperature range. All $M$ *vs.* $T$ curves are measured following the ZFC-FC-FW protocol.

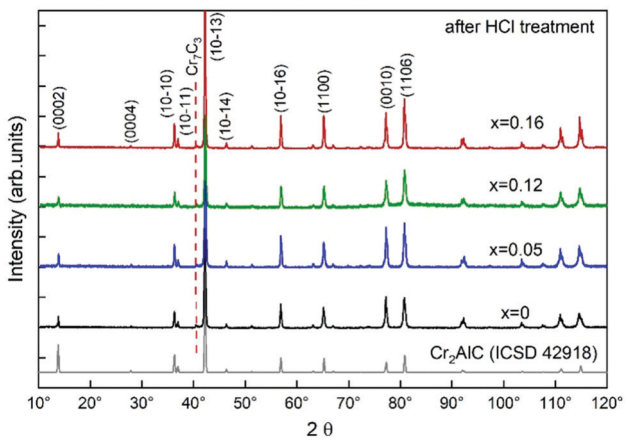


Fig. 3 XRD patterns of $(Cr_{1-x}Mn_x)_2AlC$ MAX-phase powders with Mn amounts of $x$ = 0–0.16 after 20 min of chemical treatment in 10% of HCl.

side phases, whose volume fraction is too marginal to be distinguished by XRD, SEM or TEM, but have a reasonably high magnetization.

Hysteresis loops at $T$ = 3 K of the $(Cr_{0.84}Mn_{0.16})_2AlC$ MAX-phase sample before and after the purification are shown in the inset of Fig. 5a. Chemical treatment changes the response from ferromagnetic with a saturation magnetization of 4.9 emu $g^{-1}$, a remanent magnetization of 0.8 emu $g^{-1}$ and a coercive field of 600 Oe to mainly paramagnetic behavior with a very small ferromagnetic component. The preservation of a small ferromagnetic component is clear from the evident opening of hysteresis loops that was observed for all studied samples in the whole range of temperatures, even after the purification. The magnetization at $H$ = 90 kOe decreases by more than 50% and the pronounced opening of the loop disappears. The remaining ferromagnetic component in the same sample exhibits a 99% lower remanent magnetization of 0.008 emu $g^{-1}$ and a coercive field of 150 Oe. Thus, chemical treatment removes the main ferromagnetic components (side phases) from the MAX-phase samples. However, a small residual component remains which can be either attributed to the MAX-phase itself or another trace amount of side phases which are not removed during chemical treatment. However, the structural methods above could not identify any other ferromagnetic side phase. The magnetization values of $(Cr_{0.84}Mn_{0.16})_2AlC$ MAX phase before chemical treatment is almost 5 times higher as compared with bulk $(Cr_{0.85}Mn_{0.15})_2AlC$[27] produced by microwave heating and spark plasma sintering. This is possibly due to the difference in phase composition of the samples, in particular number of secondary phases, produced by different techniques. At the same time, the magnetization of $(Cr_{0.84}Mn_{0.16})_2AlC$ MAX phase obtained in our work is 1–2 orders of magnitude lower than those previously reported by Mockute *et al.*[28] for $(Cr_{0.8}Mn_{0.2})_2AlC$ thin film. This we attribute to the higher solubility of Mn in $Cr_2AlC$ epitaxial films prepared by physical vapor deposition techniques which could strongly affect the magnetism.

Further, we investigated the temperature-dependent magnetization after chemical treatment. In Fig. 5b, $M$ *vs.* $T$ curves show no splitting in H = 100 Oe along the ZFC/FC/FW protocol. One clear transition remains close to $T$ = 42 K, which is inherent for all the Mn-containing samples from the whole series. The transition temperature changes only slightly with increasing Mn content unlike the magnetization $M$ which increases by a factor of 40 between $x$ = 0 and $x$ = 0.16. The shape of the presented curves is similar to a previous report for samples of the same composition but lower doping.[27] More details become visible as compared to preliminary results investigating samples with various side phases up to 50 vol%. In this case a high magnetic field (50 kOe) was applied, which can lead to converted magnetic transitions in the MAX phase due to the presence of side phases with high magnetization.[25] The observed magnetic ordering temperature of about 42 K has been attributed to a $Cr_{3-x}Mn_xO_4$ spinel side phase for the $(Cr,Mn)_2GaC$ MAX-phase.[35] It is likely that such oxide phase also forms in the present case and its amount rises with increasing Mn content. The relative content of this side phase is, however, lower than the XRD detection limit (<1 vol%). At this point, problems in the magnetic characterization show up. Phase pure samples are essential to determine the magnetic properties of MAX-phases which generally show a small magnetic response. To proof long-range magnetic order in MAX-phases, the rigorous purification is mandatory. Even if XRD suggests phase pure samples, some trace amounts may falsify the magnetic characterization at low temperature. Therefore, it is important to cover a wide temperature range in $M$ *vs.* $T$ measurements and apply a more detailed analysis as we will show below.

Except for the low temperature side-phase-related feature around 42 K, the curves mainly demonstrate paramagnetic $M$–$T$-dependencies (see the inset in Fig. 5b). All the curves possess rather constant behavior in the temperature range from 100 K to 800 K within the sensitivity limit of the PPMS device. A higher Mn content in the MAX-phase leads to a larger, almost constant magnetization. However, even at a Mn doping level of $x$ = 0.16 we do not observe any hints for long range magnetic order in the MAX-phase. All samples still exhibit an overall paramagnetic behavior as defined by the paramagnetic susceptibility:

$$\chi(T) = \frac{C}{T} + \chi_P$$

where the first term describes the temperature dependence of the Langevin contribution following the Curie law with the Curie constant $C$, and $\chi_P$ is the temperature-independent Pauli paramagnetic susceptibility often found in MAX-phases. Thus $\chi{\cdot}T$ *vs.* $T$ plots show a linear behavior in the regime of Pauli paramagnetism while the ordinate's intercept is the Curie constant.

Fig. 6a shows $\chi{\cdot}T$ *vs.* $T$ curves for our samples, which were calculated from the data in Fig. 5b. As expected, the feature at low temperatures due to trace amount $Cr_{3-x}Mn_xO_4$ exhibits a peak in this representation for all Mn containing samples. However, above this transition $\chi{\cdot}T$ rises almost linearly as expected for Pauli paramagnetism. We linearly fitted the data from 100 K to 300 K. The extracted temperature-independent paramagnetic component as function of doping level is shown

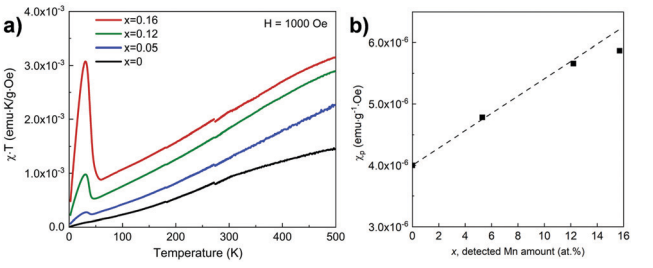


Fig. 6 (a) $\chi{\cdot}T$ *vs.* $T$ dependences for $(Cr_{1-x}Mn_x)_2AlC$ MAX-phase samples with $x$ = 0, 0.05, 0.12 and 0.16 in $H$ = 1000 Oe; (b) Pauli paramagnetic component $\chi_P$ as function of Mn content in the $(Cr_{1-x}Mn_x)_2AlC$ MAX-phase. The small kink at about 270 K is due to the temperature stabilization.

 

in Fig. 6b. The susceptibility for the $(Cr_{1-x}Mn_x)_2AlC$ MAX-phases is on the order of $10^{-6}$ emu $g^{-1}$ $Oe^{-1}$ which is the usual range for Pauli paramagnets and rises linearly up to $x = 0.12$ upon substituting Mn for Cr. This is originated from the higher filling of the conduction band with the $3d^5$ electrons of Mn as compared to $3d^4$ electrons of Cr. At highest Mn content, the results suggest the saturation of the temperature-independent component. This can possibly be associated to a solubility limit of Mn incorporation to the $Cr_2AlC$ parental MAX-phase as previously suggested.[31] An alternative way supporting the validity of the above approach is shown in Fig. S2 (ESI†) where we plot the high field susceptibility as function of temperature. The values were calculated from the linear fitting of *M vs. H* curves for the chemically treated samples in high fields – from 80 to 90 kOe. Besides the spinel side phase at low temperatures we obtain a $T^{-1}$-decreae as expected for Langevin paramagnets while the temperature-independent Pauli component provides an upshift of the curves with increasing Mn doping suggesting the coexistence of both paramagnetic components. Remarkably, the parental $Cr_2AlC$ MAX-phase is pure Pauli paramagnet as published before.[36] The value of the magnetic susceptibility, obtained for this compound in the present work, nicely matches the previously reported data for the same composition.[27] Similar values in these two cases, taking into account the absence of the purification procedure in ref. 27, is not surprising as for $Cr_2AlC$ chemical treatment makes almost no impact on the magnetic signature. The above analysis excludes ferromagnetic order in $(Cr_{1-x}Mn_x)_2AlC$ with Mn doping up to $x = 0.16$.

## Conclusions

A series of $(Cr_{1-x}Mn_x)_2AlC$ MAX-phase samples with nominal Mn doping $x = 0$, 0.1, 0.2 and 0.25 was successfully synthesized by arc melting. Comprehensive studies performed by XRD, SEM and EDX reveal good quality MAX-phases with the coexistence of secondary phases in particular at higher Mn doping levels. We demonstrate the successful chemical treatment of an antiperovskite secondary phase, resulting in phase pure $(Cr_{1-x}Mn_x)_2AlC$ MAX-phases with actual Mn amounts of $x = 0$, 0.05, 0.12, and 0.16 as judged by XRD, SEM, STEM and EDX. Magnetic characterization of the phase pure Mn doped samples between 2 K to 800 K allows to conclude that even at the highest Mn doping the MAX-phase is still paramagnetic with co-existing Pauli and Langevin contributions. A ferromagnetic feature observed at low temperature (up to 50 K) is attributed to a trace amount of $Cr_{3-x}Mn_xO_4$ spinel remaining after the purification.

## Conflicts of interest

There are no conflicts to declare.

## Acknowledgements

This work was supported by the Deutsche Forschungsgemeinschaft (DFG) within CRC/TRR 270, project B02 (Project-ID 405553726). K. S. acknowledges German-Russian Interdisciplinary Science Center (G-RISC) for the provided mobility grant that supported the present work. K. S. also acknowledges 5 top 100 Academic Excellence Project of the Russian Ministry of Science and Higher Education for the provided financial support. M. F. acknowledges co-funding by the government of the Russian Federation (agreement No. 075-15-2019-1886).

## References

1 M. W. Barsoum, *Prog. Solid State Chem.*, 2000, **28**(1–4), 201–281.
2 H. Rohde and H. Kudielka, *Cryst. Mater.*, 1960, 114.
3 W. Jeitschko, H. Nowotny and F. Benesovsky, *Monatsh. Chem.*, 1963, **94**(4), 672–676.
4 M. Sokol, V. Natu, S. Kota and M. W. Barsoum, *Trends Chem.*, 2019, **1**(2), 210–223.
5 M. Naguib, M. Kurtoglu, V. Presser, J. Lu, J. Nui, M. Heon, L. Hultman, Y. Gogotsi and M. W. Barsoum, *Adv. Mater.*, 2011, **23**(37), 4248–4253.
6 Y. Gogotsi and B. Anasori, *ACS Nano*, 2019, **13**(8), 8491–8494.
7 M. Griseri, B. Tunca, S. Huang, M. Dahlqvist, J. Rosen, J. Lu, P. O. Å. Persson, L. Popescu, J. Vleugels and K. Lambrinou, *J. Eur. Ceram. Soc.*, 2020, **40**(5), 1829–1838.
8 B. Tunca, T. Lapauw, R. Delville, D. R. Neuville, L. Hennet, D. Thiaudiere, T. Ouisse, J. Hadermann, J. Vleugels and K. Lambrinou, *Inorg. Chem.*, 2019, **58**, 6669–6683.
9 H. Ding, Y. Li, J. Lu, K. Luo, K. Chen, M. Li, P. O. Å. Persson, L. Hultman, P. Eklund, S. Du, Z. Huang, Z. Chai, H. Wang, P. Huang and Q. Huang, *Mater. Res. Lett.*, 2019, **7**(12), 510–516.
10 T. Cabioc'h, P. Eklund, V. Mauchamp and M. Jaouen, *J. Eur. Ceram. Soc.*, 2012, **32**, 1803–1811.
11 M. Dahlqvist and J. Rosen, *Nanoscale*, 2020, **12**, 785.
12 M. Dahlqvist, A. Petruhins, J. Lu, L. Hultman and J. Rosen, *ACS Nano*, 2018, **12**(8), 7761–7770.
13 A. S. Ignason, M. Dahlqvist and J. Rosen, *J. Phys.: Condens. Matter*, 2016, **28**, 433003.
14 K. A. Papadopoulou, A. Chroneos, D. Parfitt and S.-R. G. Christopoulos, *J. Appl. Phys.*, 2020, **128**, 170902.
15 L. Verger, V. Natu, M. Carey and M. W. Barsoum, *Trends Chem.*, 2019, **1**(7), 656–669.
16 A. S. Ignason, A. Petruhins, M. Dahlqvist, F. Magnus, A. Moscute, B. Alling, L. Hultman, I. A. Abrikosov, P. O. A. Persson and J. Rosen, *Mater. Res. Lett.*, 2014, **2**, 89–93.
17 I. P. Novoselova, A. Petruhins, U. Wiedwald, A. S. Ingason, T. Hase, F. Magnus, V. Kapaklis, J. Palisaitis, M. Spasova, M. Farle, J. Rosen and R. Salikhov, *Sci. Rep.*, 2018, **8**, 2637.
18 S. Lyaschenko, O. Maximova, D. Shevtsov, S. Varnakov, I. Tarasov, U. Wiedwald, J. Rosen, S. Ovchinnikov and M. Farle, *J. Magn. Magn. Mater.*, 2021, **528**, 167803.
19 Q. Tao, J. Lu, M. Dahlqvist, A. Mockute, S. Calder, A. Petruhins, R. Meshkian, O. Rivin, D. Potashnikov, E. N. Caspi, H. Shaked, A. Hoser, C. Opagiste, R.-M. Galera, R. Salikhov, U. Wiedwald, C. Ritter, A. R. Wildes,

B. Johansson, L. Hultman, M. Farle, M. W. Barsoum and J. Rosen, *Chem. Mater.*, 2019, **31**, 2476–2485.
20 R. Salikhov, R. Meshkian, D. Weller, B. Zingsem, D. Spoddig, J. Lu, A. S. Ingason, H. Zhang, J. Rosen, U. Wiedwald and M. Farle, *J. Appl. Phys.*, 2017, **121**, 163904.
21 R. Salikhov, A. S. Semisalova, A. Petruhins, A. S. Ingason, J. Rosen, U. Wiedwald and M. Farle, *Mater. Res. Lett.*, 2015, **3**(3), 156–160.
22 O. Rivin, E. N. Caspi, A. Pesach, H. Shaked, A. Hoser, R. Georgii, Q. Tao, J. Rosen and M. W. Barsoum, *Mater. Res. Lett.*, 2017, **5**(7), 465–471.
23 M. Dahlqvist, B. Alling, I. A. Abrikosov and J. Rosen, *Phys. Rev. B: Condens. Matter Mater. Phys.*, 2011, **84**(2), 220403.
24 M. Dahlqvist, B. Alling and J. Rosen, *J. Phys.: Condens. Matter*, 2015, **27**, 095601.
25 K. V. Sobolev, K. K. Kolincio, A. Emelyanov, A. Mielewczyk-Gryń, M. Gazda, M. Roman, A. Pazniak and V. Rodionova, *J. Magn. Magn. Mater.*, 2020, **493**, 165642.
26 H. Li, S. Li, H. Mao and Y. Zhou, *Adv. Appl. Ceram.*, 2017, **116**(3), 165–172.
27 C. M. Hamm, J. D. Bocarsly, G. Seward, U. I. Kramm and C. S. Birkel, *J. Mater. Chem. C*, 2017, **23**(5), 5700–5708.
28 A. Mockute, P. O. A. Persson, F. Magnus, A. S. Ignason, S. Olafsson, L. Hultman and J. Rosen, *Phys. Status Solidi*, 2014, **8**(5), 420–423.
29 K. Sobolev, M. Gorshenkov, P. Manfrinetti, D. Peddis, A. Pazniak and V. Rodionova, *Ceram. Int.*, 2021, **47**(15), 21069–21076.
30 K. Sobolev, A. Pazniak, O. Shylenko, V. Komanicky, A. Provino, P. Manfrinetti, D. Peddis and V. Rodionova, *Ceram. Int.*, 2020, **47**(6), 7745–7752.
31 A. Mockute, J. Lu, E. J. Moon, M. Yan, B. Anasori, S. J. May, M. W. Barsoum and J. Rosen, *Mater. Res. Lett.*, 2014, **3**(1), 16–22.
32 A. S. Ignason, A. Mockute, M. Dahlqvist, F. Magnus, S. Olafsson, U. D. Arnalds, B. Alling, I. A. Abrikosov, B. Hjörvarsson, P. O. A. Persson and J. Rosen, *Phys. Rev. Lett.*, 2013, **110**, 195502.
33 Q. Z. Tao, C. F. Hu, S. Lin, H. B. Zhang, F. Z. Li, D. Qu, M. L. Wu, Y. P. Sun, Y. Sakka and M. W. Barsoum, *Mater. Res. Lett.*, 2014, **2**(4), 192–198.
34 A. Kenmotsu, T. Shinohara and H. Watanabe, *J. Phys. Soc. Jpn.*, 1972, **32**(2), 377–381.
35 A. Maniv, A. P. Reyes, S. K. Ramakrishna, D. Graf, A. Huq, D. Potashnikov, O. Rivin, A. Pesach, Q. Tao, J. Rosen, I. Felner and I. Felner, *J. Condens. Matter Phys.*, 2020, **33**, 025803.
36 Z. Liu, T. Waki, Y. Tabata and H. Nakamura, *Phys. Rev. B: Condens. Matter Mater. Phys.*, 2014, **89**, 054435.

 